KfK 4940
Oktober 1991

Evaluation of R-curves in Ceramic Materials Based on Bridging Interactions

T. Fett, D. Munz
Institut für Materialforschung

Kernforschungszentrum Karlsruhe

KERNFORSCHUNGSZENTRUM KARLSRUHE
Institut für Materialforschung

KfK 4940

Evaluation of R-curves in ceramic materials based on bridging interactions

T. Fett, D. Munz

Kernforschungszentrum Karlsruhe GmbH, Karlsruhe

Kernforschungszentrum Karlsruhe GmbH
Postfach 3640, 7500 Karlsruhe 1

ISSN 0303-4003

Evaluation of R-curves in ceramic materials based on bridging interactions

Abstract

In coarse-grained alumina the crack growth resistance increases with increasing crack extension due to crack-border interactions. The crack shielding stress intensity factor can be calculated from the relation between the bridging stresses and the crack opening displacement. The parameters of this relation can be obtained from experimental results on stable or subcritical crack extension. Finally the effect of the R-curve on the behaviour of components with small cracks is discussed.

R-Kurveneffekte durch Rißflankenwechselwirkung in Keramiken

Kurzfassung

Keramische Werkstoffe - insbesondere grobkörniges Al_2O_3 - zeigen einen R-Kurveneffekt, der durch Wechselwirkung zwischen den Rißflanken verursacht ist. Es wird gezeigt, wie sich die R-Kurven aus den Wechselwirkungskräften herleiten lassen. Die Parameter des Kraftgesetzes werden aus experimentellen Literaturergebnissen bestimmt. Abschließend wird der Einfluß der R-Kurve auf das Festigkeits- und Lebensdauerverhalten von Bauteilen mit natürlichen Rissen betrachtet.

Table of Contents

1. Introduction

Coarse-grained Al_2O_3 shows an R-curve behaviour which is characterised by an increase in crack growth resistance with increasing crack extension [1]-[10]. It was demonstrated experimentally [2],[3] that this effect is caused by crack-border interactions in the wake of the advancing crack. Recently, the crack-surface interactions have been detected in-situ under the electron microscope [11],[12]. The bridging interactions were observed mainly on large grains.

Crack shielding by crack-border interaction is not only effective in a test involving increasing load. Also under constant load with subcritical crack growth the crack-border interaction affects the observed crack growth rate.
The stress intensity factor acting at the crack tip $K_{I\,tip}$ can be written as

$$K_{I\,tip} = K_{I\,appl} - K_{Ibr} \tag{1}$$

where $K_{I\,appl}$ is calculated from the external load, neglecting crack-border interaction, and $K_{I\,br}$ is caused by the compressive bridging stresses.
In the first part of the paper an appropriate bridging stress relation is established. Then the general influence of the bridging stresses on the R-curve behaviour of macro-cracks is studied for stable and subcritical crack growth. In three examples of application the parameters of the bridging law are determined from literature results. After describing the general R-curve behaviour of small cracks, a procedure is presented that allows to determine the bridging parameters of natural cracks.

2. Calculation of R-curves

2.1 *The bridging stress relation*

The bridging stresses are dependent on the crack opening displacement δ. Mai and Lawn [13] proposed a relation

$$\sigma_{br,grain} = \begin{cases} \sigma_0(1-\delta/\delta_0)^m & \text{for } \delta/\delta_0 < 1 \\ 0 & \text{for } \delta/\delta_0 > 1 \end{cases}, \quad m = 0,1,2,... \tag{2}$$

that is shown in fig.1.

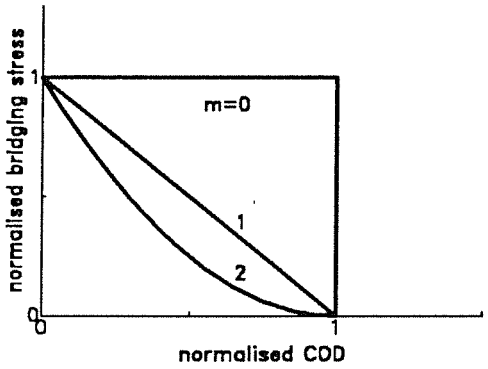

Fig.1 Stress-displacement relations for a single grain $\sigma_{br}/\sigma_0 = f(\delta/\delta_0)$.

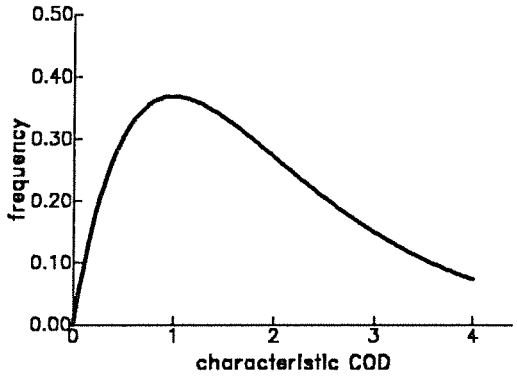

Fig.2 Distribution of the characteristic COD-value δ_0 (abscissa normalised: δ_0/δ_{00}).

It is assumed that the characteristic displacement for which the bridging stresses vanish is proportional to the grain size. On account of grain size distribution, also the characteristic displacement is distributed.
It is assumed that the distribution density of δ_0 is a Γ-distribution, as represented in fig.2.

$$f(\delta_0) = \frac{1}{\delta_{00}} \frac{\delta_0}{\delta_{00}} \exp(-\delta_0/\delta_{00}) \tag{3}$$

Other Γ-distributions are considered in the Appendix.
The macroscopically averaged bridging stresses result from

$$\sigma_{br,aver} = \int_0^\infty \sigma_{br,grain}\, f(\delta_0)\, d\delta_0 \tag{4}$$

For the most appropriate Γ-distribution, eq.(3), the following averaged bridging stress relations result:

$$\sigma_{br,aver} = \sigma_0\, g(\delta/\delta_{00}) \tag{5}$$

with

$$g(z) = (1+z)\, \exp(-z) \qquad \text{for} \quad m = 0 \tag{5.1}$$

$$g(z) = \exp(-z) \qquad \text{for} \quad m = 1 \tag{5.2}$$

$$g(z) = (1 - z)\ \exp(-z) + z^2 \mathbf{Ei}(z) \qquad \text{for} \quad m = 2 \tag{5.3}$$

where **Ei** is the exponential integral defined by

$$\mathbf{Ei}(x) = \int_x^{\infty} \frac{e^{-t}}{t}\, dt \quad , \quad x > 0 \tag{5.4}$$

available in most computer libraries. These bridging laws are shown in fig.3.

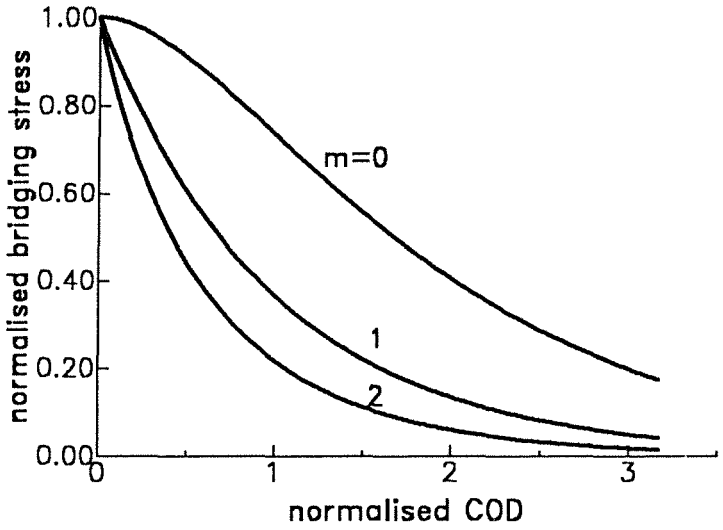

Fig.3 Influence of the parameter m in eq.(2) on the averaged bridging stress.

These relations ensure a continuously decreasing effect of crack-border interaction with decreasing displacement. Especially the mostly applied case $m = 1$ is used in the subsequent calculations.

2.2 Calculation of the bridging stress intensity factor

A test specimen with a crack may be loaded by an external load, which leads to a stress distribution $\sigma_{appl}(x)$ at the location of the crack in the uncracked component. The geometrical quantities of such a crack are explained in fig.4.

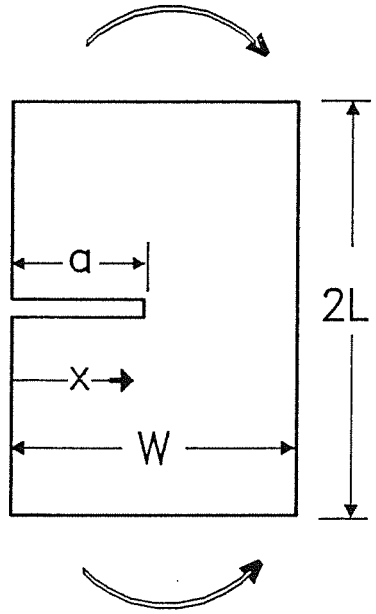

Fig.4 Specimen with a crack under bending load.

In case the material exhibits a bridging zone with crack-surface interactions, the total stress is the sum of the applied stress and the bridging stress σ_{br} , i.e.

$$\sigma_{total}(x) = \sigma_{appl}(x) - \sigma_{br}(x) \tag{6}$$

It is convenient to use a minus sign in eq.(6) and positive values of σ_{br}. These stresses are responsible for the stress intensity factor, which is given in the representation of the weight function [14]

$$K_I = \int_0^a h(\frac{x}{a}, \frac{a}{W})\sigma(x)\, dx \tag{7}$$

The total displacements of the crack surface can be easily derived by the relation existing between crack surface displacements, weight function and stress intensity factor as proposed by Rice [15]

$$h = \frac{H}{K_I}\frac{\partial \delta}{\partial a} \tag{8}$$

with H=E for plane stress and H=E/(1-ν^2) for plane strain.
Integration of this formula yields the crack-surface displacements δ caused by the stress σ [16]

$$\delta(x) = \frac{1}{H}\int_0^a \int_{\max(x,x')}^a h(a',x)h(a',x')\sigma(x')da'dx' \tag{9}$$

where x is the coordinate with the displacement computed and x' is the location where the stress σ acts. Equation (9) can also be derived from the procedure of Paris [17] based on Castiglianos Theorem. A detailed description is given in the Appendix of Tadas' Handbook [18].
The stress intensity factors describing the R-curve behaviour can be obtained in the following way:

1. The total crack surface displacements according to the total stress, eq.(6), result as

$$\delta = \frac{1}{H}\int_0^a \int_{\max(x,x')}^a h(a',x)h(a',x')(\sigma_{appl} - \sigma_{br})da'dx' = \delta_{00} g^{-1}(\sigma_{br}/\sigma_0) \tag{10}$$

   where g^{-1} is the inverse of the function defined by eq.(5).
   The solution of the integral equation (10) provides the distribution of the bridging stresses as a function of the stresses applied.

2. The related bridging stress intensity factor $K_{I\,br}$ results from eq.(7) as

$$K_{I\,br} = \int_0^a h(\frac{x}{a}, \frac{a}{W})\sigma_{br}(x)\, dx \tag{7.1}$$

3. and the applied stress intensity factor $K_{I\,appl}$ as

$$K_{I\,appl} = \int_0^a h(\frac{x}{a}, \frac{a}{W})\sigma_{appl}(x)\,dx \tag{7.2}$$

4. Finally, the crack tip stress intensity factor $K_{I\,tip}$ is given by eq.(1).

The solution of the integral equation (10) can be determined by several methods. The simplest one is the iterative approximation. In the first step, the applied stress σ_{appl} is introduced in the integrand of eq.(10) yielding the crack surface displacement field δ_{appl} . A first approximation of the bridging stresses is obtained by introducing δ_{appl} in the bridging stress law. The bridging stresses obtained are then introduced once more in eq.(10) and the procedure is repeated as long as the bridging displacements are constant.
In principle the evaluation of eq.(10) using successive approximation needs much computer time. In order to reduce the computation effort, special strategies are given in the Appendix. The simplest one is to use tabulated solutions of the previous procedure in normalised form. These data can easily be interpolated by cubic splines.
For the numerical calculations the weight function derived in [19] is applied

$$h_I = \sqrt{\frac{2}{\pi a}}\,\frac{1}{\sqrt{1-x/a}\,(1-a/W)^{3/2}}\left[(1-\frac{a}{W})^{3/2} + \sum A_{\nu\mu}(1-x/a)^{\nu+1}(\frac{a}{W})^{\mu}\right] \tag{11}$$

with the coefficients $A_{\nu\mu}$ given in Table 1.

	$\mu=0$	1	2	3	4
$\nu=0$	0.4980	2.4463	0.0700	1.3187	-3.067
1	0.54165	-5.0806	24.3447	-32.7208	18.1214
2	-0.19277	2.55863	-12.6415	19.763	-10.9860

Table 1. Coefficients for eq.(11)

2.3 *General results*

In fig.5 results of calculations for a crack with an initial relative crack size (e.g. a saw notch) of $a_0/W = 0.5$ ($m = 1$, $\delta'_{00} = 1$) under bending are represented as $K_{I\,tip}$ vs. $K_{I\,appl}$ for several actual crack lengths a/W. In this figure, the stress intensity factors are normalised with respect to the maximum bridging stress σ_0 and the specimens width W as

$$K'_I = \frac{K_I}{\sigma_0\sqrt{W}} \tag{12}$$

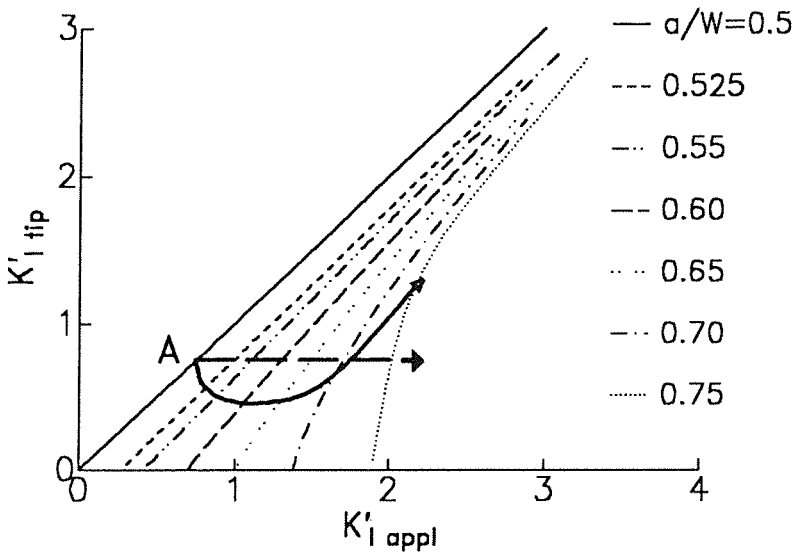

Fig.5 Stress intensity factor $K'_{I\,tip}$ as a function of applied stress intensity factor $K'_{I\,appl}$ in a normalised representation (bending, $\delta'_{00}=1$, $a_0/W=0.5$).

In the tables of section 8 a number of stress intensity factors have been collected for several relative crack lengths a/W and several values of δ_{00} as defined in eq.(4). These values are normalised by

$$\delta'_{00}=\frac{H}{\sigma_0 W}\,\delta_{00} \tag{13}$$

The tables allow to determine by simple interpolations the stress intensity factors for a range of relevant values of $K_{I\,appl}$, a/W and δ_{00}.

2.3.1 Constant load tests

The representation of the stress intensity factor, fig.5, allows to describe crack extension tests under different loading conditions. In fig.5 crack propagation in a constant load test under subcritical crack growth conditions is illustrated by the solid line for $\sigma/\sigma_0=0.4$ and $\delta'_{00}=1$. The curve starts at point A corresponding to $K_{I\,appl}=K_{I\,tip}=\sigma\sqrt{a_0}\,Y$. With increasing crack length, first the crack-tip stress intensity factor $K_{I\,tip}$ decreases and after reaching a minimum value, $K_{I\,tip}$ increases monotonically.
The applied stress intensity factor $K_{I\,appl}$ is plotted in fig.6 versus the crack extension $\Delta a/W$. The $K_{I\,appl}$-$\Delta a/W$-curve increases monotonically. This is self-evident since for constant stress the stress intensity factor

$$K_{I\,appl}=\sigma_{appl}\sqrt{a}\;Y(a/W) \tag{14}$$

reflects only the increase in the product $\sqrt{a}\,Y$ with crack extension, and this quantity is not a material property, but depends only on the geometric data a, a/W.

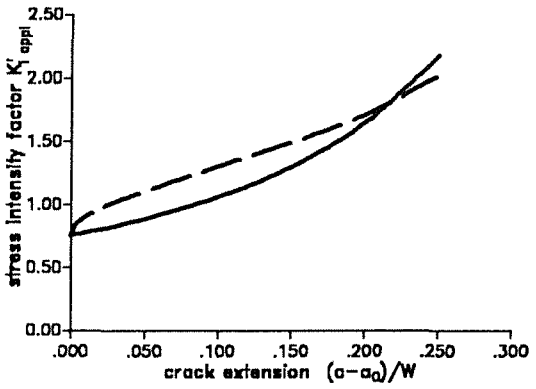

Fig.6 Applied stress intensity factor for crack extension under constant load (solid line) and constant stress intensity factor $K_{I\,tip}$ (dashed line); $a_0/W = 0.5$.

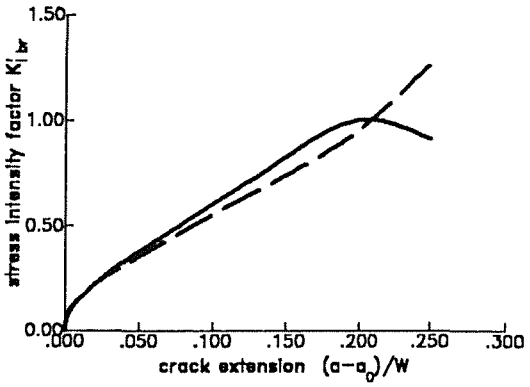

Fig.7 Bridging stress intensity factor as a function of crack extension (solid curve: constant load test, dashed curve: test with constant $K'_{I\,tip}$).

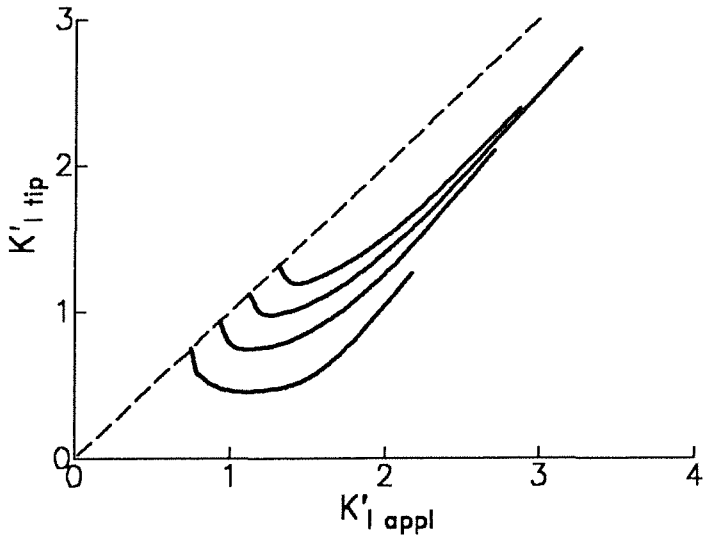

Fig.8 Development of the crack-tip stress intensity factor $K'_{I\,tip}$ in constant load tests.

The bridging stress intensity factor developing with increasing crack length is traced in fig.7 as a solid line. A comparison between the two R-curve representations $K_{I\,br} = f(\Delta a)$ and $K_{I\,appl} = f(\Delta a)$ shows the superiority of $K_{I\,br} = f(\Delta a)$ since this representation reflects the material behaviour. Constant load tests for several initial stress intensity factors K_{Ii} are shown in fig.8. The influence of the initial stress intensity factor on the R-curve can be seen from fig.9. It is evident that the R-curve is more pronounced for low values of applied stress.

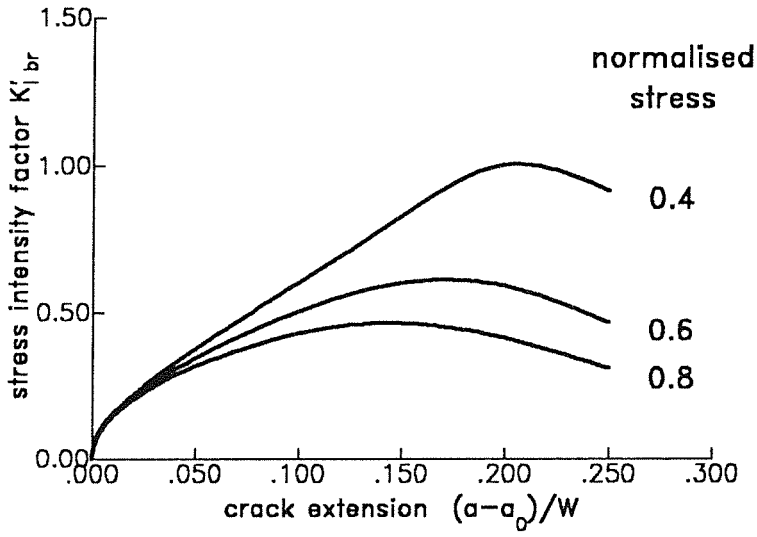

Fig.9 Development of the R-curve stress intensity factor $K'_{I\,br}$ in constant load tests (normalised stress $= \sigma/\sigma_0$).

2.3.2 Crack extension with constant crack-tip stress intensity factor

In this section tests with constant stress intensity factor $K_{I\,tip}$ are considered. Such tests are difficult to perform. One possibility would be to perform tests with constant crack growth rate. Results are presented here to show the differences to the tests with constant stress. Crack extension with constant stress intensity factor $K_{I\,tip}$ (e.g. stable crack propagation with $K_{I\,tip} = K_{I0} = const.$) is described by the dashed horizontal line (fig.5). The related $K_{I\,appl}$-vs. Δa-curve is also entered in fig.6. At the beginning of crack extension, the curve is approximately square-root shaped in accordance with the literature (e.g. [20]). Also for this type of crack propagation, the R-curve representation $K_{I\,br} = f(\Delta a)$ is introduced in fig.7 (dashed line). For little crack extension this curve deviates hardly from the curve obtained under constant load conditions. Significant differences in the shapes of the R-curves become obvious for large crack extensions.
R-curves for crack propagation at $K_{I\,tip} = \text{const.}$ are shown in fig.10 for different values of $K_{I\,tip}$. It becomes obvious that the R-curve depends on the level of $K_{I\,tip}$.
The bridging stress intensity factor $K_{I\,br}$ is plotted in fig.11 vs. $\Delta a/W$. In this representation the dependency on $K_{I\,tip}$ becomes more obvious. As can be seen from figs.6,7,9,10 and 11, the bridging stress intensity factor $K_{I\,br}$ shows a square-root shaped increase for small crack extensions. This can easily be understood. If the crack extension is small compared with the initial notch depth $\Delta a = a - a_0 \ll a_0$, the displacements δ_{total}, δ_{appl} and δ_{br} are also small within the whole range $a_0 \leq x \leq a$. In this case, it holds $\delta \ll \delta_{00}$ and, consequently, $\sigma_{br} \simeq \sigma_0$.
In this special case the application of the weight function yields the bridging stress intensity factor

$$K_{Ibr} = \sqrt{\frac{8a}{\pi}}\,\sigma_0 \left\{ \sqrt{1 - a_0/a} + \sum A_{\mu\nu} \frac{1}{2\nu + 3} \frac{(a/W)^{\mu}}{(1 - a/W)^{3/2}} (1 - a_0/a)^{\nu + 3/2} \right\} \tag{15}$$

Since for $\Delta a \to 0$ in eq.(15) only the first term in brackets contributes to the bridging stress intensity factor, it results

$$K_{I\,br} = \sigma_0 \sqrt{\frac{8\Delta a}{\pi}} \tag{16}$$

and the square-root shaped increase in the bridging stress intensity factor with crack extension becomes obvious.

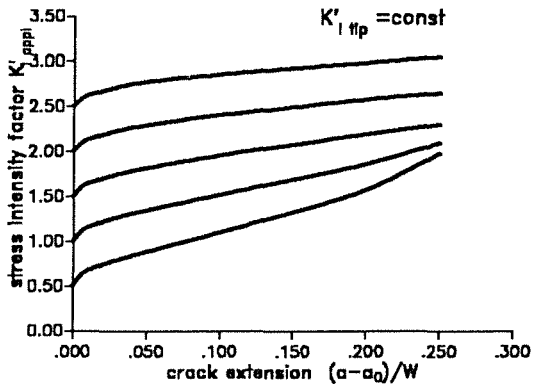

Fig.10 "R-curves" for crack extension with constant crack-tip stress intensity factors $K_{I\,tip}$.

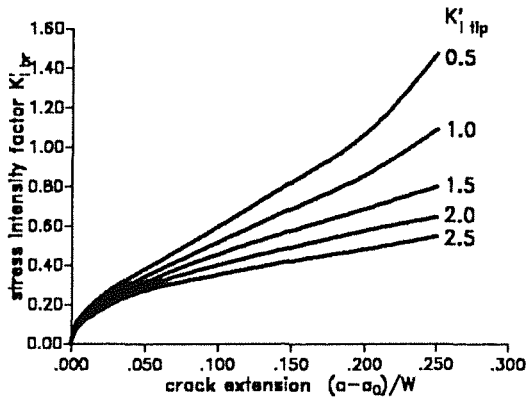

Fig.11 Development of the bridging stress intensity factor $K_{I\,br}$ for crack extension tests with constant crack-tip stress intensity factor $K_{I\,tip}$.

3. Determination of bridging stress parameters from literature results

In this chapter, the weight-function based procedure described above is applied to determine the parameters (σ_0, δ_{00}) of the bridging stress law from experimental data available in the literature. For the evaluation eq.(5.2) is assumed to be valid.

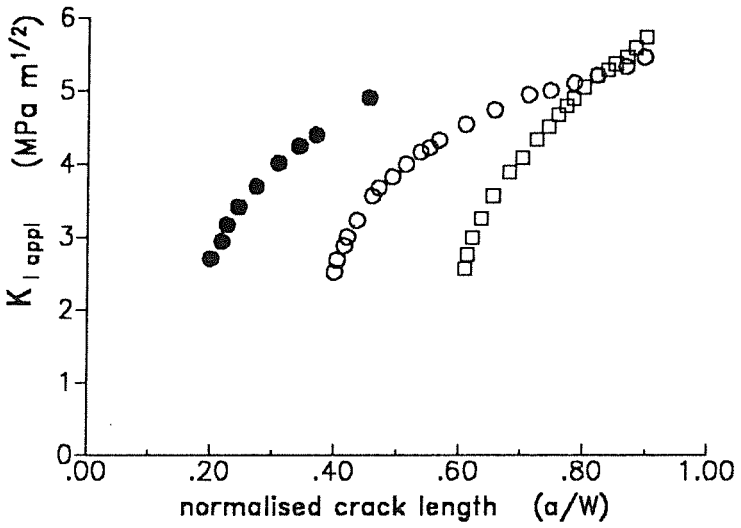

Fig.12 R-curves for coarse-grained Al_2O_3 based on measurements of Steinbrech and Schmenkel [4].

3.1 Stable crack propagation

First stable crack propagation is considered. Figure 12 shows a set of R-curves for 99.8%-Al_2O_3 with a mean grain size of $\simeq 16\mu$m [4]. The original data expressed by energy release rates were converted by

$$K_{I\,appl} = [GE/(1-\nu^2)]^{1/2} \tag{17}$$

(E = 360GPa, $\nu = 0.22$) into applied stress intensity factors $K_{I\,appl}$. The crack-tip stress intensity factor $K_{I\,tip}$ in the stable crack growth test is given by the initial value of $K_{I\,appl}$ at $\Delta a = 0$. Due to the approximately square-root-shaped R-curves for $\Delta a \to 0$, this value can hardly be measured in a stable crack growth test. Therefore, the value of K_{I0} has also to be considered to be an unknown parameter.

In order to determine the unknown parameters σ_0, δ_{00}, K_{I0}, a least-squares procedure was applied for the R-curve with $a_0/W = 0.4$. The procedure is described in the following steps:

1. Starting with a first estimation of the parameters the normalised stress intensity factor $K'_{I\,tip}$ is computed by

$$K'_{I\,tip} = \frac{K_{I\,tip}}{\sigma_0\sqrt{W}} \tag{18}$$

2. Parabolic interpolation of table 9.4 using bicubic splines for a/W, $K'_{I\,tip}$ and cubic splines for δ'_{00} yields $K'_{I\,appl}$ and hence the calculated stress intensity factor

$$K_{I\,appl,calc} = K'_{I\,appl}\,\sigma_0\sqrt{W} \tag{19}$$

In this way, one obtains the calculated R-curve

$$K_{I\,appl,calc} = f(a/W,\ \sigma_0,\ \delta_{00})$$

for the actual parameter set.

3. The least-squares routine compares the calculated R-curve with the experimental R-curve and determines the sum of squares according to

$$S^2 = \sum (K_{I\,appl,calc} - K_{I\,appl,exp})^2 \tag{20}$$

The routine changes the parameter set (σ_0, δ_{00}, K_{I0}) as long as a minimum of S^2 is reached. So the best parameter set in least-squares terms is determined. For the practical use the authors applied the Harwell-Routine VA02A.

As a result of this procedure it was found:

$$\delta'_{00} = 0.5\ ,\ K'_{I\,tip} = 0.69\ ,\ K_{I0} = 2.4\text{MPa}\sqrt{\text{m}}$$

and with $W = 7$mm

$$\sigma_0 = 42MPa\ ,\ \delta_{00} = 0.41\mu m$$

The fitting curve corresponding to these parameters is plotted in fig.13 as a solid line. Using this parameter set also the R-curves for $a_0/W = 0.2$ and 0.6 were calculated. The results are plotted in fig.13 as dashed lines. The agreement is excellent for $a_0 = 0.6$, and also for $a_0/W = 0.2$ the experimental results can be well described. But for large crack extension deviations are evident.
Since the bridging stress parameters are known, the crack surface profile results from eq.(10). Figure 14 shows the crack profile for the crack with $a_0/W = 0.4$ after a crack propagation of $\Delta a/W = 0/0.1/0.2$ and 0.3.

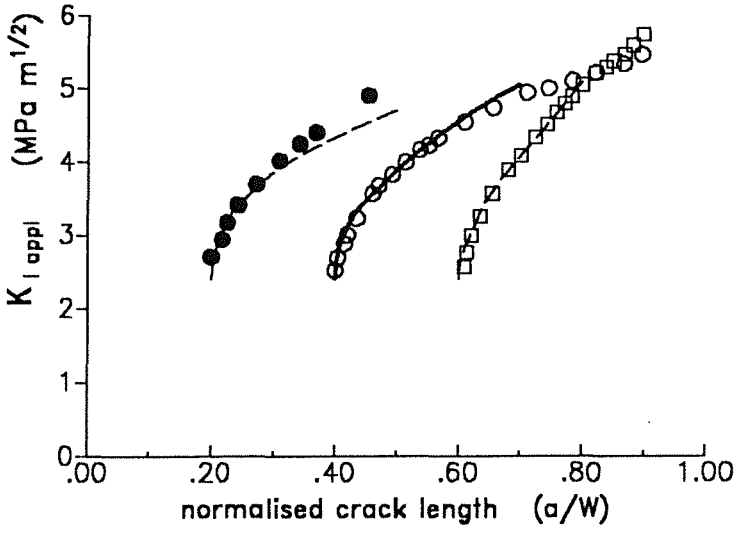

Fig.13 R-curves of fig.12 compared with curves calculated with the parameters from the least-squares procedure; (solid curve: fitted R-curve, dashed curves: predicted R-curves).

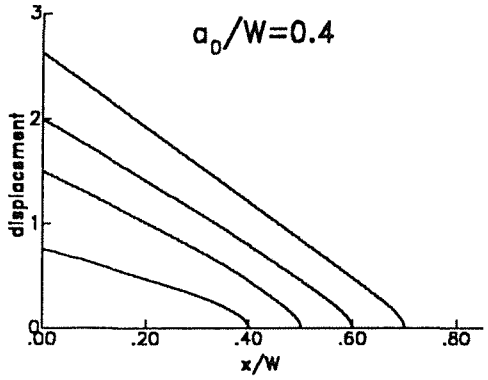

Fig.14 Crack surface profiles according to fig.13 (displacements in μm).

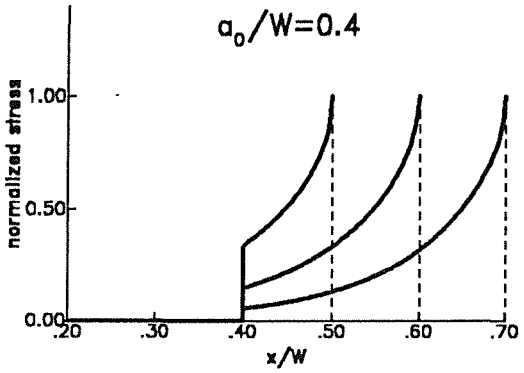

Fig.15 Bridging stresses for cracks with different crack extensions: (lines as in fig.14).

The crack surface profiles exhibit the square-root-shaped near-tip displacements, which are directly proportional to the crack-tip stress intensity factor $K_{I\,tip}$. The corresponding distribution of the bridging stresses $\sigma_{br}(x)$ is shown in fig.15.
It should be mentioned in this context, that the presented procedure based on the fracture-mechanical weight function does not require any additional assumption to be made on a special crack opening profile, as for example applied in a J-integral evaluation performed by Steinbrech et al [21].

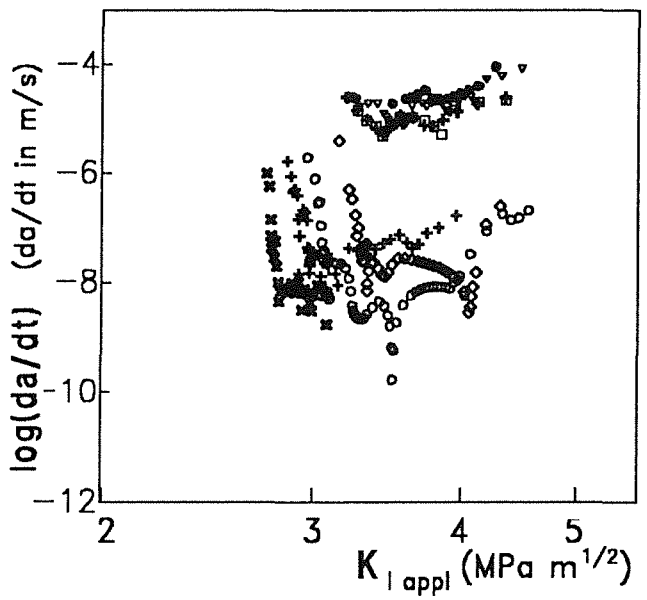

Fig.16 $v - K_I$ –curves for specimens with macrocracks from static bending tests (material I) [9]; (K_{Ii}=2.72/2.96/3.06/2.82/3.20/3.21/3.25$MPa\sqrt{m}$).

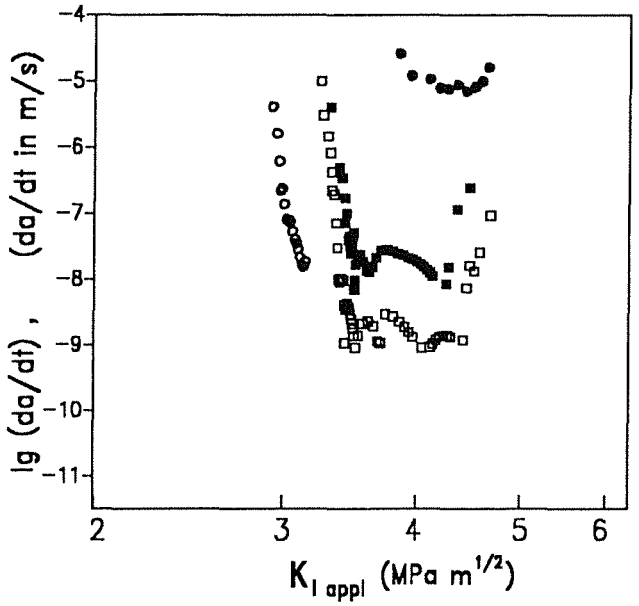

Fig.17 $v - K_I$ –curves for specimens with macrocracks from static bending tests (material II) [9]; ($K_{Ii} = 2.93/3.25/3.32/3.85 MPa\sqrt{m}$).

3.2 *Subcritical crack extension*

A second possibility of determining the parameters of eq.(5.2) is the evaluation of subcritical crack growth measurements. Results of crack growth measurements for alumina from specimens with macrocracks are reported in [9]. Two commercially available materials were investigated:

- material I : 99.6%-Al_2O_3 $K_{Ic} = 3.3 MPa\sqrt{m}$, average grain size 20μm.
- material II: 99.6%-Al_2O_3 (hipped) $K_{Ic} = 4 MPa\sqrt{m}$; this material shows an inhomogeneous grain size distribution with a mean grain size of 3.2μm and maximum grains of $\simeq$25μm size.

The results reported in [9] were obtained with single-edge notched specimens, 3.5x4.5x50mm in size, loaded in three-point bending with a constant load. The notch in the center of the specimen was prepared with a diamond saw. The notch depth was 2.245$\pm$0.01mm, the notch width 50μm.
In fig.16 and fig.17 $da/dt - K_{I\,appl}$-curves are plotted for different stresses applied. Two types of $da/dt - K_I$-curves can be seen. First, a decrease of the crack growth rate with increasing crack length and therefore increasing $K_{I\,appl}$ is obvious. The crack growth rate drops by several orders of magnitude within a small amount of crack extension. After a large range with a nearly constant crack growth rate the crack growth rate increases until final fracture. For the lowest K_{Ii} for both materials crack arrest was observed.
Whilst in case of stable crack extension the value $K_{I\,tip}$ is known, the crack-tip stress intensity factor changes during crack propagation in constant load tests.
In order to determine the parameters σ_0, δ_{00} from constant load tests, also a least-squares procedure is applied. The treatment is outlined for the special case that the subcritical crack growth is described by a power law relation

$$v = \frac{da}{dt} = AK_I^n = A^*(K_I/K_{Ic})^n \tag{21}$$

- The procedure starts with an estimated initial combination of parameters (σ_0, δ_{00}, A^*, n). For any data point ($K_{I\,appl}$, a/W) the crack tip stress intensity factor $K_{I\,tip}$ is calculated, and using eq.(21) the subcritical crack growth rate v_{calc} is calculated.

- The calculated and the measured crack growth rates v_{meas} are intercompared and the sum of squares is determined by

$$S^2 = \sum \left(\log(v_{calc}) - \log(v_{meas}) \right)^2 \qquad (22)$$

- Further treatment by a least-squares procedure is similar to that for stable crack propagation apart from the fact that now a set of 4 parameters are determined.

The result of calculation is:

$$\text{material I}: \quad \sigma_0 = 46.4MPa, \quad \delta_{00} = 0.95\mu m, \quad \log A^* = -2.97, \quad n = 25$$

$$\text{material II}: \quad \sigma_0 = 88.8MPa, \quad \delta_{00} = 0.224\mu m, \quad \log A^* = -0.7, \quad n = 25$$

In earlier investigations the subcritical crack growth behaviour of natural cracks was determined for material I [22] and material II [23] by application of a modified lifetime method [24] ignoring possible R-curve effects. The result was $n = 38$ for material I and $n = 20$ for material II. The discrepancies in the n-values for the macro-cracks may be caused either by fundamental differences in the subcritical crack growth behaviour of natural, small cracks compared with artificial macro-cracks or/and by intolerable influences of the R-curve on the evaluation procedure for the natural cracks.

To check the accuracy of the parameters determined (σ_0, δ_{00}, A^*, n), the least-squares sums S^2 - normalised to the minimum value S^2_{min} - are plotted in fig.18 for a number of power law exponents n. The dashed line represents δ'_{00} and the dash-dotted curve shows σ_0.

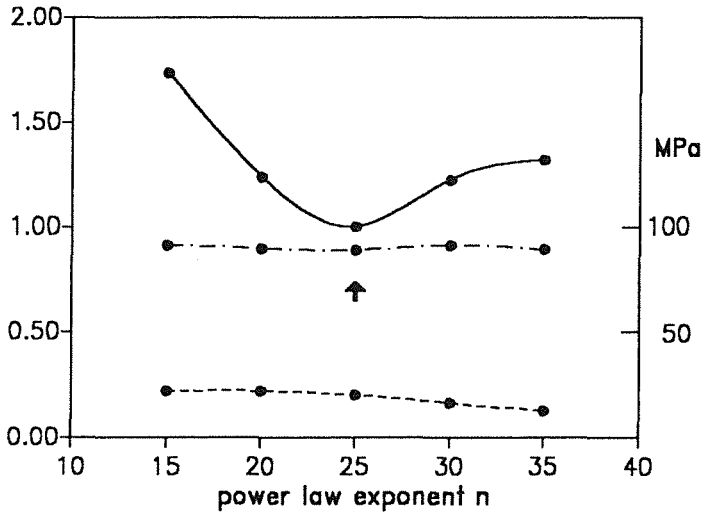

Fig.18 Least-squares results for fixed exponents n; S^2/S^2_{min} (solid curve, left hand scale), δ'_{00} (dashed curve, left hand scale), σ_0 (dash-dotted, right hand scale): material II.

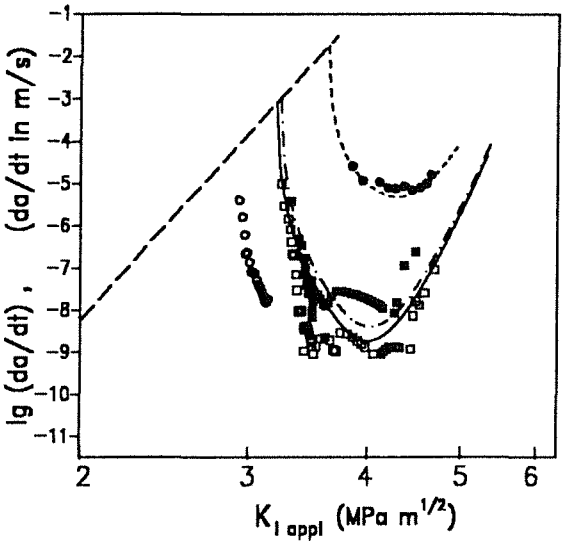

Fig.19 $v - K_{I\,appl}$ –curves for material II calculated with the fitted parameter set (dashed straight line: $v = f(K_{I\,tip})$).

In fig.19 the $v - K_{I\,appl}$ –curves - calculated with the bridging parameters of material II - are plotted for several initial stress intensity factors K_{Ii}. The dashed straight line describes the power law relation $v = AK_{tip}^{n}$. Finally, fig.20 shows the R-curve calculated with the fitted material data.

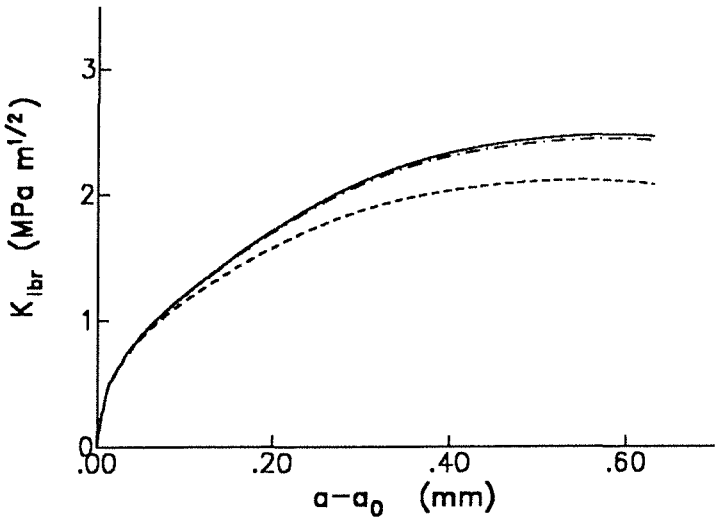

Fig.20 R-curves for material II calculated with the fitted parameter set (lines as in fig.19).

A comparison of the $\sigma - \delta$ –relations, obtained for the three materials is given in fig.21.

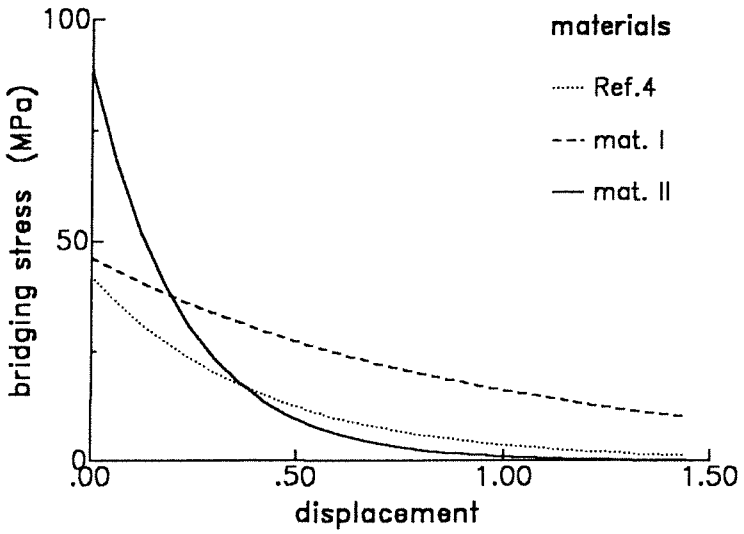

Fig.21 Bridging stress relations for the three materials investigated.

4. R-curve for natural cracks

In this section it is assumed that the bridging stresses determined with macro-cracks can be applied also to natural cracks. It is of special interest how the bridging stresses affect the strength and the lifetimes of specimens with natural flaw population. The natural cracks are modelled by semi-circular surface cracks ignoring special surface influences, i.e. by a half of an embedded circular crack. As illustrated in fig. 22, the initial crack size is a_0 and the actual crack size is a. The displacements due to the radial stress distribution $\sigma(r)$ are described by [25]

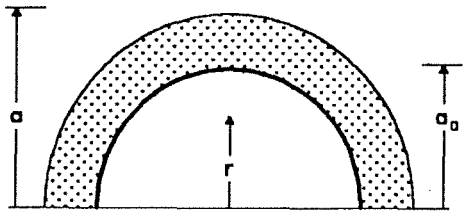

Fig.22 Semi-circular crack.

$$\delta(r) = \frac{4(1-\nu^2)}{\pi E}\, a \int_{\rho}^{1} \frac{1}{\sqrt{x^2-\rho^2}} \left[\int_{0}^{x} \frac{\rho\, \sigma\, d\rho}{\sqrt{x^2-\rho^2}} \right] dx \quad ; \quad \rho = r/a \tag{23}$$

where x is a dimensionless integration variable. The related stress intensity factor is given by

$$K_I = \frac{2}{\sqrt{\pi a}} \int_{0}^{a} \frac{r\, \sigma(r)\, dr}{\sqrt{a^2-r^2}} \tag{24}$$

4.1 Analytical solutions for special cases

The crack surface displacement under homogeneously distributed stress $\sigma = \sigma_{appl} = const.$ is

$$\delta_{appl} = \frac{4(1-\nu^2)}{\pi E}\, \sigma_{appl} \sqrt{a^2-r^2} \tag{25}$$

and the stress intensity factor

$$K_{I\,appl} = \frac{2}{\sqrt{\pi}}\, \sigma_{appl} \sqrt{a} \tag{26}$$

The maximum displacement (occurring at $r=0$) results as

$$\delta_{appl\,r=0} = \frac{4(1-\nu^2)}{\pi E}\, \sigma_{appl}\, a = \frac{2(1-\nu^2)}{\sqrt{\pi}\, E}\, K_{I\,appl} \sqrt{a} \tag{27}$$

For a crack with $a = 100\mu m$ and $E = 360$GPa we obtain a maximum displacement when $K_{I\,appl}$ reaches K_{I0}. With a value of $K_{I0} = 3$MPa$\sqrt{m}$ - typical of coarse-grained Al_2O_3 - it results

$$\delta_{appl,max} = 0.09\ \mu m$$

If we compare this limit value with the characteristic displacements δ_{00} and if we keep in mind that

1. the displacements decrease from the crack origin to the crack-tip, and
2. the bridging stresses will reduce the crack opening,

we can realize that the relevant crack surface displacements are small compared with the values δ_{00}. This will at least hold for material I. Consequently, one can approximate

$$\sigma_{br} \simeq \sigma_0$$

For material II, where δ_{00} is of the same order of magnitude as the displacements in the bridging zone, this approximation will lead to an upper limit case for the R-curve of the natural cracks. With this simplification made, the bridging stress intensity factor results from eq.(24)

$$K_{I\,br} = \frac{2}{\sqrt{\pi a}}\,\sigma_0\sqrt{a^2 - a_0^2} \tag{28}$$

The crack surface displacement due to the bridging stresses is given by [26]

$$\delta_{appl} = \delta^* \frac{4(1-\nu^2)\,a\,\sigma_0}{\pi E} \tag{29}$$

with

$$\delta^* = \int_{r/a}^{a_0/a} \frac{x\,dx}{\sqrt{x^2 - (r/a)^2}} + \int_{a_0/a}^{1} \frac{x - \sqrt{x^2 - (a_0/a)^2}}{\sqrt{x^2 - (r/a)^2}}\,dx \qquad \text{for} \quad r < a_0 \tag{30a}$$

$$\delta^* = \int_{a/r}^{1} \frac{x - \sqrt{x^2 - (a_0/a)^2}}{\sqrt{x^2 - (r/a)^2}}\,dx \qquad \text{for} \quad r > a_0 \tag{30b}$$

or in an analytically integrated form

$$\delta^* = \sqrt{1-(r/a)^2}\,\sqrt{1-(a_0/a)^2} - \frac{a_0}{a}\left[\mathbf{E}(r/a_0) - E(\arcsin a_0/a, r/a_0)\right] \quad \text{for} \quad r < a_0 \tag{30c}$$

and

$$\delta^* = \sqrt{1-(r/a)^2}\,\sqrt{1-(a_0/a)^2}$$

$$-\frac{r}{a}\left[\mathbf{E}(a_0/r) - E(\arcsin r/a, a_0/r) - (1 - a_0{}^2/r^2)(\mathbf{K}(a_0/r) - F(\arcsin r/a, a_0/r))\right] \quad \text{for} \quad r > a_0 \tag{30d}$$

where F and E are the first and second elliptical integrals and $\mathbf{K}$ and $\mathbf{E}$ are the corresponding complete elliptical integrals. In this context, it should be mentioned that the solution given by Sneddon [25], namely

$$\delta^* = \sqrt{1-(r/a)^2}\,\sqrt{1-(a_0/a)^2} \tag{31}$$

is wrong ([26]).

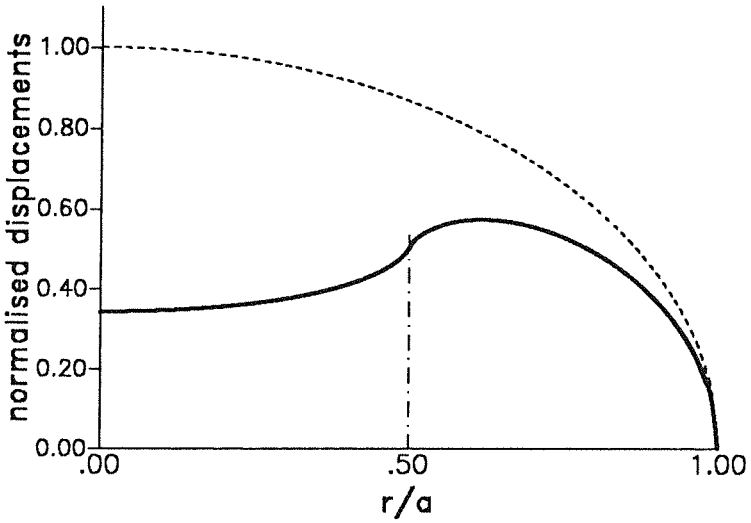

Fig.23 Displacements due to bridging stresses (normalised displacement = $-\delta^*$) for $a_0/a = 0.5$ (solid curve) and $a_0/a = 0$ (dashed curve).

Figure 23 shows the displacements caused by the bridging stresses in a normalised representation. In fig.24 the R-curve according to eq.(28) is plotted for the natural cracks. In a strength test only a small part of this curve will be covered. The points of instability where the strength is reached (material I: 220MPa, materal II: 370MPa) are marked by solid circles.

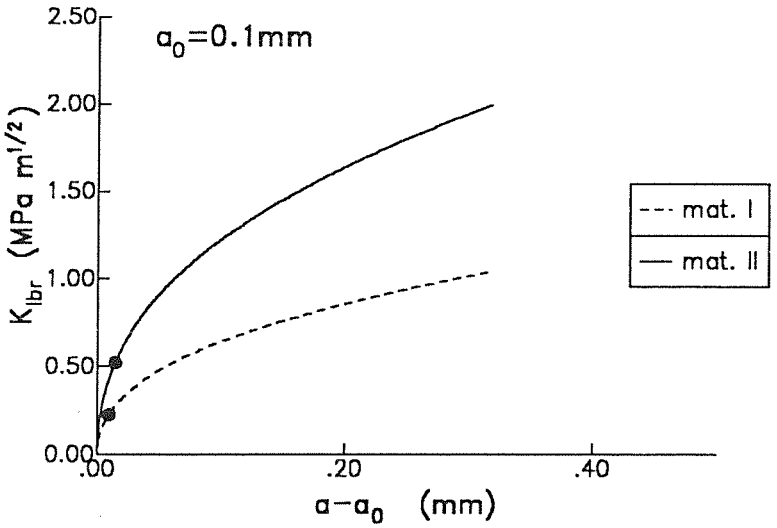

Fig.24 R-curves for the natural cracks (circles: location of failure).

4.2 *Influence of bridging stresses on strength*

The critical stress σ_c (the strength) results from the two conditions

$$K_{I0} = K_{I\,appl} - K_{I\,br}(\Delta a) \quad , \quad \left(\frac{\partial K_{I\,appl}}{\partial a}\right)_{\sigma=const=\sigma_c} = \frac{d K_{I\,br}}{d(\Delta a)} \tag{32}$$

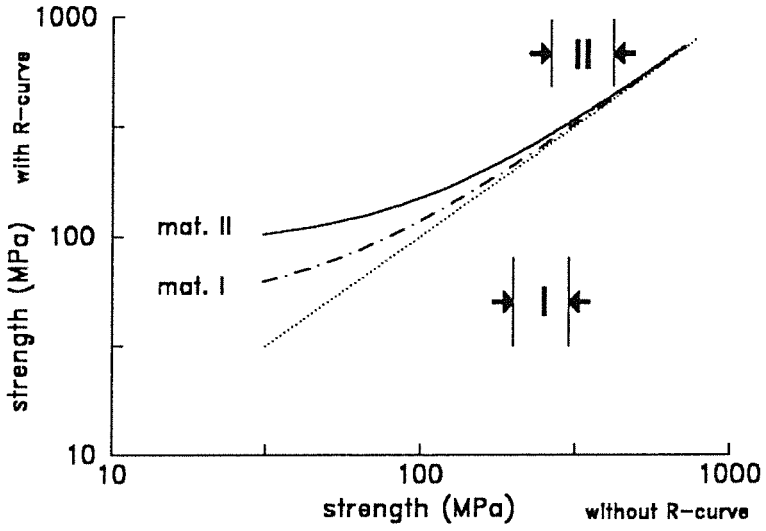

Fig.25 Influence of bridging stresses on the inert strength.

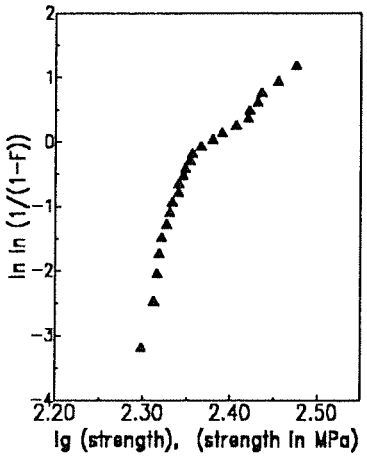

Fig.26 4-point-bending strength of material I [22].

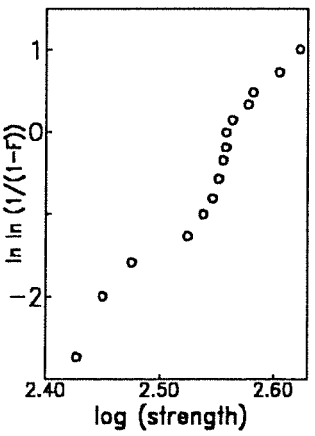

Fig.27 4-point-bending strength of material II [27].

Figure 25 represents the strength influenced by the bridging stresses as a function of the strength when no bridging effect occurs. The range of experimentally determined strength data according

to figs. 26 and 27 is introduced in fig.25. The influence of the macroscopic R-curve on the strength of specimens with natural flaw population is not strong which can be concluded from fig.25.

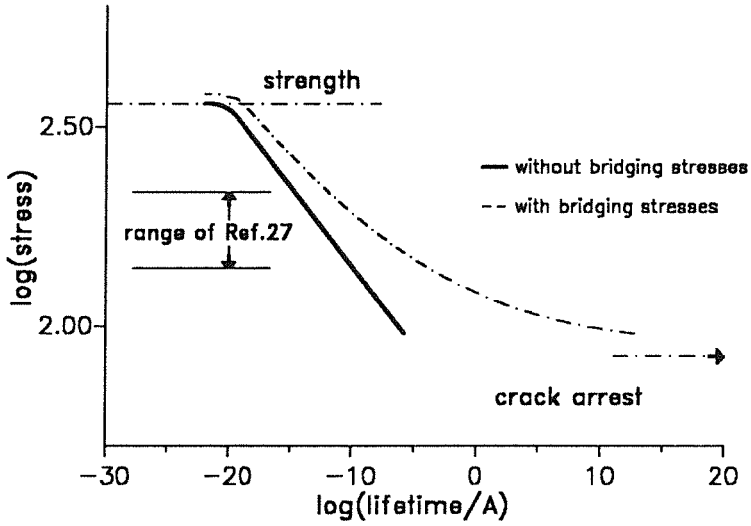

Fig.28 Influence of bridging stresses on the lifetime in static tests (material II).

4.3 *Influence of bridging stresses on lifetimes*

The lifetime t_f in a static test performed with the stress σ results in

$$t_f = \int_{a_0}^{a_c} \frac{da}{v} = \frac{1}{A} \int_{a_0}^{a_c} \frac{da}{[\sigma Y \sqrt{a} - K_{I\,br}]^n} \tag{33}$$

where a_o is the initial value of the crack length a and a_c is the crack length at failure. Under sub-critical crack growth conditions the crack size at failure a_c can be derived from a failure condition analogous to eq.(32) for the applied stress σ.
In fig.28 the influence of the bridging stresses on the lifetimes is illustrated. The comparison between the lifetimes in the presence of bridging stresses and lifetimes in the absence of bridging stresses shows longer lifetimes as a consequence of the bridging stresses. Also a lower slope of the curve with bridging stresses is evident. This will lead to an increased exponent of the power law $t_f \propto \sigma^{-1}$. The slightly different strength values can be seen also in fig.28.

4.4 *A procedure to determine bridging stresses for natural cracks*

It cannot be excluded that bridging behaviour of natural cracks may deviate from the behaviour of macro-cracks. Therefore, it is desirable to determine the bridging stress relation for natural cracks.
In case that the lifetimes are affected by the bridging stresses, it should - in principle - be possible to determine these stresses from lifetime measurements. A possible procedure - based on strength and lifetime measurements in static tests - is described below:

1. At the beginning of the procedure a least-squares routine provides a set of parameters A,n for a power law description of subcritical crack growth and σ_0, δ_{00}, m for a three-parametric bridging relation (e.g. eqs.(5.1-5.3)).

2. For each measured strength value σ_{cv} the related initial crack size a_{iv} is determined from the failure conditions in strength tests

$$K_{I\,appl} = \sigma_{cv} Y \sqrt{a_{cv}} = K_{I0} + K_{I\,br}|_{a_{cv} - a_{0v}} \qquad Y \simeq 2/\sqrt{\pi}$$
$$\left(\frac{\partial K_{I\,appl}}{\partial a_{cv}} \right)_{\sigma = const} = \frac{d K_{I\,br}}{d a_{cv}} \tag{34}$$

3. Lifetime computations:

   a. Calculation of the final crack length a_c in a constant load test using eq.(32) for the stress occurring in the tests.
   b. In the next step the integral equation - resulting by combination of eqs.(5) and (23) - has to be solved:

$$\log \frac{\sigma}{\sigma_0} + \frac{4(1-\nu^2)}{\pi E \delta_{00}} a \int_{\rho}^{1} \frac{1}{\sqrt{x^2 - \rho^2}} \left[\int_{0}^{x} \frac{\rho\, \sigma\, d\rho}{\sqrt{x^2 - \rho^2}} \right] dx = 0 \tag{35}$$

   The solution of this integral equation can be determined by successive approximation. The result is the radial distribution of the bridging stresses over the crack.
   c. Equation (24) then provides the bridging stress intensity factor $K_{I\,br}$.
   d. Now, all information is available to evaluate the lifetime relation

$$t_{f\,calculated} = \frac{1}{A} \int_{a_0}^{a_c} \frac{da}{[\sigma Y \sqrt{a} - K_{I\,br}]^n} \tag{36}$$

4. The calculated lifetimes are then compared with the measured ones and the sum of squares is determined as

$$S^2 = \Sigma (\log t_{f\,calculated} - \log t_{f\,measured})^2 \tag{37}$$

5. In the next step the parameter set is changed systematically and the procedure starts again from point 1 with these new parameters.

6. The procedure is repeated as long as the squares S^2 get minimum.

The result is the best parameter set for description of the v-K_I-curve and bridging relation. An appropriate least-squares computer subroutine is, for instance, the Harwell routine VA02A.

4.5 Calculations of normalised bridging stress intensity factors for small cracks

Lifetime calculations according to the procedure proposed in section 6.4 require the solution of eq.(35) for any crack growth increment *da* during evaluating of eq.(36). In order to reduce the effort in determination of the bridging stress intensity factors, eq.(35) has been solved numerically for several values of the parameters δ_{00}, a_0/a, $K_{I\,tip}$. Since the displacements near the crack-tip ($\rho \to 1$) are proportional to $\sqrt{1-\rho}$ and the stresses are proportional to $\exp(-\delta/\delta_{00})$ it is recommended to fit the stresses in terms of the coordinate ρ as

$$\sigma_{br}/\sigma_0 = \exp\left[\sum_{\nu=0}^{N} A_\nu (1-\rho)^{\nu+1/2}\right] \tag{38}$$

The presented calculations were performed with $N = 6$. The resulting stress intensity factors were normalised by

$$K_I{}^* = K_I \frac{1}{2\sigma_0}\sqrt{\pi/a} \tag{39}$$

and entered in Table 9.6. The characteristic displacements δ_{00} are normalised as

$$\delta_{00}^* = \frac{\pi H}{4a\sigma_0}\delta_{00} \tag{40}$$

5. Conclusions

In conclusion, the R-curve effect caused by bridging stresses between the crack surfaces has been analysed by application of the fracture-mechanical weight function. Exponential relations describing the macroscopically averaged bridging stresses have been derived, and the related R-curves have been calculated for conditions of subcritical and stable crack propagations. Crack growth data from the literature were used to determine the parameters of the bridging relation by a least-squares procedure.

In order to reduce computation work, tables are provided with the applied stress intensity factors $K_{I\,appl}$ for given values of the crack-tip stress intensity factors $K_{I\,tip}$, relative crack length a/W, and the parameter δ'_{00}.

By use of the bridging stresses obtained in macro-crack tests the influence on strength and lifetime could be studied also for small natural cracks.

6. References

[1] H. Hübner, W. Jillek, Sub-critical crack extension and crack resistance in polycrystalline alumina, J. Mater. Sci. **12**(1977)117-125.

[2] R. Knehans, R.W. Steinbrech, Memory effect of crack resistance during slow crack growth in notched Al_2O_3 bend specimens, J. Mater. Sci. Letters, **1**(1982),327-329.

[3] R.W. Steinbrech, R. Knehans, W. Schaarwächter, Increase of crack resistance during slow crack growth in Al_2O_3 bend specimens, J. Mater. Sci., **18**(1983),265-270.

[4] R. Steinbrech, O. Schmenkel, Crack-resistance curves for surface cracks in Alumina, Comm. J. Amer. Ceram. Soc. **71**(1988),C271-C273.

[5] E.K. Beauchamp, S.L. Monroe, Effect of crack-interface bridging on subcritical crack growth in ferrites, J. Amer. Ceram Soc. **72**(1989),1179-1184.

[6] D.G. Jensen, V. Zelizko, M.V. Swain, Small flaw static fatigue crack growth in Mg-PSZ, J. Mater. Sci. Letters **8**(1989),1154-1157.

[7] A. Okada, N. Hirosaki, M. Yoshimura, Subcritical crack growth in sintered silicon nitride exhibiting a rising R-curve, J. Amer. Ceram. Soc. **73**(1990),2095-2096.

[8] P.L. Swanson, C.J. Fairbanks, B.R. Lawn, Y. Mai, B.J. Hockey, Crack-interface grain bridging as a fracture resistance mechanism in ceramics: I Experimental study on alumina, J. Amer. Ceram. Soc. **70**(1987),279-289.

[9] T. Fett, D. Munz, Subcritical crack growth of macro-cracks in alumina with R-curve-behaviour, submitted to J. Amer. Ceram. Soc.

[10] G. Vekinis, M.F. Ashby, P.W.R. Beaumont, R-curve behaviour of Al_2O_3 ceramics, Acta metall. mater. **38**(1990),1151-1162.

[11] H. Frei, G. Grathwohl, New test methods for engineering ceramics - in-situ microscopy investigation, Ceramic Forum International, cfi, **67**(1991), 27-35.

[12] J. Rödel, J.F. Kelly, B.R. Lawn, In situ measurements of bridged crack interfaces in the scanning electron microscope, J. Amer. Ceram. Soc. **73**(1990),3313-3318.

[13] Y. Mai, B.R. Lawn, Crack-interface grain bridging as a fracture resistance mechanism in ceramics: II. Theoretical fracture mechanics model, J. Amer. Ceram. Soc. **70**(1987),289.

[14] H. Bückner, ZAMM **50**(1970)751.

[15] J. R. Rice, Int. J. Solids Structures **8**(1972)751-758

[16] T. Fett, D. Munz, Influence of crack-surface interactions on stress intensity factor in ceramics, J. Mater. Sci. Letters **9**(1990),1403-1406.

[17] P.C. Paris, Document D2-2195, The Boeing Company, 1957.

[18] H. Tada, "The stress analysis of cracks handbook", Del. Research Corporation (1986).

[19] T. Fett, "Stress intensity factors and weight functions for the edge cracked plate calculated by the Boundary Collocation Method", KfK-Report 4791, Kernforschungszentrum Karlsruhe, 1990.

[20] M. Sakai, J. Yoshimura, Y. Goto, M. Inagaki, R-curve behavior of a polygranular graphite: Microcracking and grain bridging in the wake region, J. Amer. Ceram. Soc. **71**(1988).

[21] R. Steinbrech, A. Reichl, W. Schaarwächter,J. Amer. Ceram. Soc. **73**(1990),2009-2015.

[22] T. Fett, D. Munz, Proc. of the 7th CIMTEC, Montecatini, Italy, 24/30 June 1990, 1827-1835.

[23] T.Fett, K. Keller, D. Munz, NAGRA, Technical Report 85-51(1985), Baden, Switzerland.

[24] T. Fett, D. Munz , Commun. of the Amer. Ceram Soc. 68,(1985) C213-C215.

[25] I.N. Sneddon, Proc. of the Royal Soc., London, A 187(1946),229.

[26] T. Fett, Crack opening displacement of a penny-shaped crack in an infinite body loaded by internal pressure over a circular area, Int. J. Fract. **20**(1982),R135-R138.

[27] T. Fett, D. Munz, Subcritical crack growth of macro- and microcracks in ceramics, Proc. of "Fracture Mechanics of Ceramics", in press, Nagoya, July 16, 1991.

7. Appendix

7.1 Other Γ-distributions

If the distribution of the characteristic COD-value δ_0 is given by a Γ-distribution with n≥1 (fig.A1)

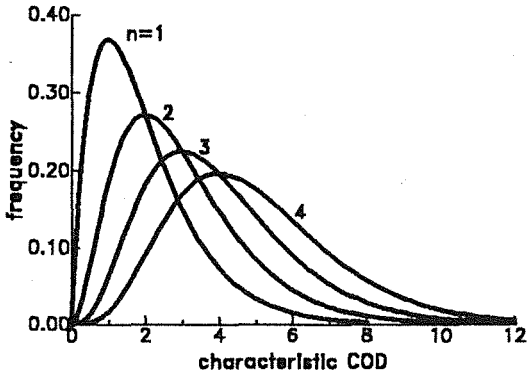

Fig.A1 Γ-distributed characteristic CODs.

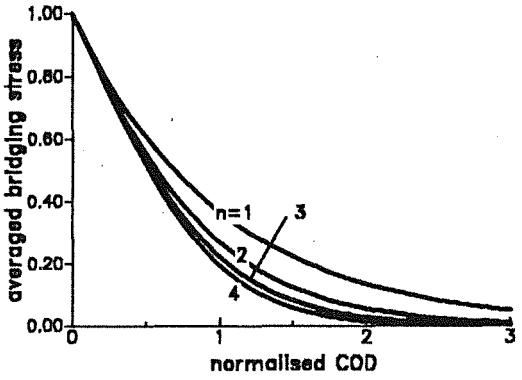

Fig.A2 Influence of characteristic COD-distribution on shape of averaged bridging stress for m=1.

one obtains

$$f(z) = \frac{1}{\Gamma(n+1)} z^n e^{-z} \qquad z = \delta_0/\delta_{00} \tag{A1}$$

For integer n and $m = 1$ the averaged bridging stresses become

$$\sigma_{br,aver}/\sigma_0 = \int_{\delta/\delta_{00}}^{\infty} \left(1 - \frac{\delta}{\delta_{00}} \frac{1}{z}\right) f(z)\, dz = e^{-\delta/\delta_{00}} \sum_{\nu=0}^{n} \frac{\nu}{n\,\Gamma(n-\nu+1)} \left(\frac{\delta}{\delta_{00}}\right)^{n-\nu} \tag{A2}$$

The special case, eq.(3), is easily obtained by setting n=1. In fig.A2 the averaged bridging stresses are shown for n=1,..,4. All curves show the dominant influence of the exponential term in eq.(A2)

7.2 Practical treatment in evaluation of eq.(10)

A numerical evaluation of the double integral, eq.(10), with sufficient accuracy is very expensive in terms of computer time. A significant reduction of the efforts needed is proposed here.

7.2.1 Description of bridging stresses by polynomials

In terms of stress intensity factors, eq.(9) can be expressed by

$$\delta = \frac{1}{H}\int_x^a h(x,a')K_I(a')da' \tag{A3}$$

In order to determine the displacements caused by the bridging stresses, the bridging stress intensity factor has to be introduced in eq.(A3). If the type of stress distribution is known, eq.(10) and eq.(A3) can be used conveniently. This is outlined for the case of a polynomial stress distribution near the crack tip which may be given by

$$\sigma = \sum_{n=0}^{N} C_n(x' - a_0)^n \tag{A4}$$

where a_0 is the range of the crack without crack surface interactions (i.e. the depth of the starter notch). The stress intensity factors result from eq.(5) by using the weight function in the form

$$h = \sqrt{\frac{2}{\pi a}}\sum_{\mu=0}^{M} A_\mu\left(1 - \frac{x'}{a}\right)^{\mu-1/2} \tag{A5}$$

after elementary integration as

$$K_{br} = \sqrt{\frac{2}{\pi}}\sum_{n=0}^{N} a^{n+1/2}C_n\sum_{\mu=0}^{M} A_\mu\left(1 - \frac{a_0}{a}\right)^{\mu+n+1/2}\frac{\Gamma(n+1)\Gamma(\mu+1/2)}{\Gamma(\mu+n+3/2)} \tag{A6}$$

where Γ is the Gamma-function.
This equation was used mainly in sections 3 and 4 where the numerically obtained distributions of bridging stresses were fitted with respect to eq.(A3) by polynomials up to n = 19.

7.2.2 A least-squares procedure for solving eq.(10)

In this procedure the unknown bridging stress distribution is described by a polynomial of degree N as given by eq.(A4). Introducing this set-up in eq.(9) yields the displacements δ_{br} caused by the bridging stresses σ_{br} in the form

$$\delta_{br}(x) = \sum_{n=0}^{N} C_n\delta_n(x) \tag{A7}$$

with

$$\delta_n(x) = \frac{1}{H}\int_0^a\int_{\max(x,x')}^a h(a',x)h(a',x')\,(x' - a_0)^n\,da'dx' \tag{A8}$$

If the bridging stress law is written as

$$\sigma_{br} = f(\delta) = f(\delta_{appl} + \delta_{br}) \tag{A9}$$

inversion of this relation yields the corresponding displacements as

$$\delta_{br} = f^{-1}(\sigma_{br}) - \delta_{appl} = f^{-1}\left(\sum_{n=0}^{N} C_n(x - a_0)^n\right) - \delta_{appl} \tag{A10}$$

Now eq.(10) can be written

$$f^{-1}\left(\sum_{n=0}^{N} C_n (x - a_0)^n\right) - \delta_{appl} = \sum_{n=0}^{N} C_n \delta_n \qquad (A11)$$

In a least-squares procedure the coefficients C_n are systematically changed as long as both sides of eq.(A11) are identical within a prescribed maximum error. It should be noted that in the course of the least-squares procedure the integrals $\delta_n(x)$ remain constant and numerical integration is only necessary at the beginning of the procedure.
From the resulting set of coefficients C_n the bridging stresses and by use of eq.(7) the bridging stress intensity factor are known. An effective least-squares computer routine is for instance Harwell VA02A.

8. Tables

Tables 8.1-8.5

In the following tables the normalised stress intensity factors $K'_{I\,appl} = f(\delta'_{00}, K'_{I\,tip}, a/W)$ are given for different exponents of the bridging relations according to eq.(2) and different initial crack sizes a_0/W. An additional requirement - useful for extrapolations $\delta'_{00} \to 0$ - is given by: $K'_{I\,appl} = K'_{I\,tip}$ for $\delta'_{00} = 0$.

Considering the square-root shaped dependency $K_{I\,br} \propto \sqrt{\Delta a}$ it should be recommended to calculate at first

$$F = \frac{K'_{I\,appl} - K'_{I\,tip}}{\sqrt{\Delta a}}$$

with

$$F|_{\Delta a=0} = \sqrt{8/\pi}$$

and to interpolate these values F.

The tables for m = 0/1/2 allow to interpolate also these exponents.

Table 8.6

Table 8.6 shows the normalised stress intensity factor $K^*_{I\,appl} = f(\delta^*_{00}, K^*_{I\,tip}, a_0/a)$ in the normalisations of (39) and (40) for $m = 1$ (eq.(2)).

For $a \simeq a_0$ a square-root shaped dependency occurs as a consequence of eq.(28)

$$K^*_{I\,br}|_{a_0 \to 1} = \sqrt{\frac{2\Delta a}{a}}$$

This limit behaviour should be taken into consideration for interpolations near $a_0 \simeq a$ (i.e. for $\Delta a \to 0$).

In case of $\delta^*_{00} \to \infty$ one obtains the additional *exact* data

$$K_{I\,appl}{}^* = K^*_{I\,tip} + \sqrt{1 - (a_0/a)^2}$$

and for $\delta^*_{00} \to 0$ it results

$$K_{I\,appl}{}^* = K^*_{I\,tip}$$

For values $\delta_{00}{}^* \leq 1$ it is recommended to interpolate $\delta_{00}{}^*$ directly and for $\delta_{00}{}^* \geq 1$ interpolations with respect to the reciprocal value $1/\delta_{00}{}^*$ should be preferred.

δ'_{00}	a/W	$K'_{I\,tip} = 0.$	0.25	0.50	1.00	1.50
0.25	0.500	0.00	0.25	0.50	1.00	1.50
0.25	0.525	0.28	0.52	0.76	1.24	1.71
0.25	0.550	0.42	0.65	0.88	1.33	1.77
0.25	0.600	0.71	0.89	1.07	1.43	1.83
0.25	0.650	1.01	1.11	1.21	1.49	1.85
0.25	0.700	1.30	1.31	1.32	1.53	1.87
0.25	0.750	1.44	1.44	1.44	1.58	1.89
0.5	0.500	0.00	0.25	0.50	1.00	1.50
0.5	0.525	0.27	0.52	0.77	1.26	1.75
0.5	0.550	0.42	0.66	0.91	1.39	1.86
0.5	0.600	0.71	0.95	1.17	1.59	2.01
0.5	0.650	1.06	1.26	1.43	1.78	2.14
0.5	0.700	1.51	1.62	1.73	1.95	2.24
0.5	0.750	2.05	2.05	2.05	2.13	2.33
1.0	0.500	0.00	0.25	0.50	1.00	1.50
1.0	0.525	0.27	0.52	0.77	1.27	1.76
1.0	0.550	0.41	0.67	0.92	1.41	1.90
1.0	0.600	0.72	0.97	1.21	1.68	2.14
1.0	0.650	1.08	1.32	1.54	1.97	2.39
1.0	0.700	1.58	1.78	1.97	2.32	2.67
1.0	0.750	2.29	2.41	2.53	2.75	2.99
2.0	0.500	0.00	0.25	0.50	1.00	1.50
2.0	0.525	0.28	0.52	0.77	1.27	1.78
2.0	0.550	0.42	0.67	0.92	1.42	1.91
2.0	0.600	0.72	0.97	1.22	1.71	2.19
2.0	0.650	1.10	1.34	1.58	2.06	2.53
2.0	0.700	1.60	1.84	2.07	2.51	2.94
2.0	0.750	2.37	2.57	2.78	3.15	3.51

Table 8.1:
Normalised stress intensity factor $K'_{I\,appl} = f(\delta'_{00}, K'_{I\,tip}, a/W)$
for $a_0/W = 0.5$ and $m = 0$.

δ'_{00}	a/W	$K'_{I\,tip} = 0.$	0.25	0.50	1.00	1.50
0.25	0.500	0.00	0.25	0.50	1.00	1.50
0.25	0.525	0.26	0.48	0.70	1.16	1.63
0.25	0.550	0.39	0.57	0.77	1.20	1.64
0.25	0.600	0.60	0.72	0.86	1.24	1.66
0.25	0.650	0.77	0.82	0.92	1.26	1.67
0.25	0.700	0.89	0.90	0.97	1.27	1.68
0.25	0.750	0.99	0.99	1.03	1.28	1.69
0.5	0.500	0.00	0.25	0.50	1.00	1.50
0.5	0.525	0.26	0.50	0.73	1.21	1.69
0.5	0.550	0.40	0.62	0.83	1.28	1.75
0.5	0.600	0.66	0.82	0.99	1.38	1.82
0.5	0.650	0.91	1.01	1.13	1.46	1.86
0.5	0.700	1.17	1.20	1.27	1.52	1.89
0.5	0.750	1.39	1.39	1.42	1.59	1.92
1.0	0.500	0.00	0.25	0.50	1.00	1.50
1.0	0.525	0.26	0.51	0.75	1.24	1.72
1.0	0.550	0.41	0.64	0.87	1.34	1.81
1.0	0.600	0.70	0.90	1.10	1.52	1.95
1.0	0.650	0.99	1.15	1.31	1.69	2.07
1.0	0.700	1.37	1.46	1.57	1.86	2.19
1.0	0.750	1.99	1.94	1.97	2.09	2.30
2.0	0.500	0.00	0.25	0.50	1.00	1.50
2.0	0.525	0.27	0.51	0.76	1.25	1.74
2.0	0.550	0.42	0.65	0.90	1.38	1.86
2.0	0.600	0.70	0.92	1.15	1.60	2.07
2.0	0.650	1.04	1.23	1.44	1.84	2.27
2.0	0.700	1.48	1.64	1.80	2.14	2.50
2.0	0.750	2.09	2.17	2.28	2.52	2.81

Table 8.2:
Normalised stress intensity factor $K'_{I\,appl} = f(\delta'_{00}, K'_{I\,tip}, a/W)$
for $a_0/W = 0.5$ and $m = 1$.

δ'_{00}	a/W	$K'_{I\,tip} = 0.$	0.25	0.50	1.00	1.50
0.25	0.500	0.00	0.25	0.50	1.00	1.50
0.25	0.525	0.25	0.45	0.66	1.11	1.58
0.25	0.550	0.37	0.53	0.71	1.13	1.59
0.25	0.600	0.52	0.61	0.76	1.13	1.59
0.25	0.650	0.61	0.67	0.79	1.15	1.59
0.25	0.700	0.70	0.73	0.82	1.16	2.00
0.25	0.750	0.77	0.77	0.84	1.17	2.00
0.5	0.500	0.00	0.25	0.50	1.00	1.50
0.5	0.525	0.26	0.48	0.71	1.17	1.64
0.5	0.550	0.40	0.58	0.79	1.22	1.67
0.5	0.600	0.61	0.73	0.90	1.28	1.70
0.5	0.650	0.80	0.87	0.99	1.32	1.72
0.5	0.700	0.98	1.00	1.07	1.35	1.74
0.5	0.750	1.11	1.12	1.15	1.39	1.75
1.0	0.500	0.00	0.25	0.50	1.00	1.50
1.0	0.525	0.26	0.50	0.73	1.20	1.69
1.0	0.550	0.40	0.62	0.84	1.29	1.75
1.0	0.600	0.66	0.83	1.01	1.41	1.84
1.0	0.650	0.93	1.04	1.18	1.52	1.91
1.0	0.700	1.23	1.27	1.36	1.63	1.98
1.0	0.750	1.53	1.54	1.56	1.74	2.05
2.0	0.500	0.00	0.25	0.50	1.00	1.50
2.0	0.525	0.27	0.51	0.75	1.23	1.72
2.0	0.550	0.41	0.64	0.87	1.34	1.82
2.0	0.600	0.69	0.89	1.10	1.53	1.97
2.0	0.650	1.00	1.16	1.34	1.72	2.12
2.0	0.700	1.39	1.50	1.63	1.93	2.29
2.0	0.750	1.90	1.92	1.98	2.19	2.47

Table 8.3:
Normalised stress intensity factor $K'_{I\,appl} = f(\delta'_{00}, K'_{I\,tip}, a/W)$
for $a_0/W = 0.5$ and $m = 2$.

δ'_{00}	a/W	$K'_{I\,tip} = 0.25$	0.5	0.75	1.0	1.5
0.5	0.400	0.25	0.50	0.75	1.00	1.50
0.5	0.425	0.48	0.73	0.97	1.20	1.68
0.5	0.450	0.61	0.83	1.05	1.28	1.74
0.5	0.500	0.80	0.97	1.16	1.37	1.80
0.5	0.550	0.96	1.09	1.26	1.44	1.83
0.5	0.600	1.11	1.21	1.34	1.50	1.86
0.5	0.650	1.25	1.31	1.41	1.54	1.88
0.5	0.700	1.38	1.40	1.47	1.58	1.90
1.0	0.400	0.25	0.50	0.75	1.00	1.50
1.0	0.425	0.51	0.75	0.99	1.24	1.72
1.0	0.450	0.63	0.86	1.10	1.33	1.80
1.0	0.500	0.86	1.06	1.27	1.49	1.92
1.0	0.550	1.08	1.25	1.44	1.63	2.03
1.0	0.600	1.32	1.46	1.61	1.77	2.13
1.0	0.650	1.59	1.67	1.78	1.91	2.22
1.0	0.700	1.89	1.92	1.98	2.06	2.32
2.0	0.400	0.25	0.50	0.75	1.00	1.50
2.0	0.425	0.52	0.76	1.00	1.25	1.74
2.0	0.450	0.65	0.88	1.13	1.37	1.85
2.0	0.500	0.89	1.12	1.34	1.57	2.03
2.0	0.550	1.16	1.36	1.57	1.78	2.21
2.0	0.600	1.47	1.64	1.82	2.01	2.40
2.0	0.650	1.83	1.97	2.12	2.28	2.60
2.0	0.700	2.31	2.38	2.48	2.60	2.85

Table 8.4:
Normalised stress intensity factor $K'_{I\,appl} = f(\delta'_{00}, K'_{I\,tip}, a/W)$
for $a_0/W = 0.4$ and $m = 1$.

δ'_{00}	a/W	$K'_{I\,tip} = 0.0$	0.25	0.5	0.75	1.0	1.5
0.25	0.200	0.00	0.25	0.50	0.75	1.00	1.50
0.25	0.225	0.26	0.48	0.70	0.93	1.16	1.63
0.25	0.250	0.37	0.56	0.77	0.98	1.20	1.65
0.25	0.300	0.54	0.67	0.84	1.02	1.23	1.65
0.25	0.350	0.67	0.75	0.88	1.05	1.23	1.66
0.25	0.400	0.76	0.80	0.91	1.06	1.55	1.67
0.25	0.500	0.86	0.88	0.95	1.08	1.26	1.67
0.5	0.200	0.00	0.25	0.50	0.75	1.00	1.50
0.5	0.225	0.27	0.50	0.73	0.97	1.20	1.68
0.5	0.250	0.39	0.60	0.82	1.04	1.27	1.73
0.5	0.300	0.59	0.76	0.95	1.15	1.35	1.79
0.5	0.350	0.76	0.90	1.05	1.22	1.41	1.82
0.5	0.400	0.93	1.01	1.13	1.28	1.45	1.84
0.5	0.500	1.20	1.22	1.27	1.38	1.51	1.87
1.0	0.200	0.00	0.25	0.50	0.75	1.00	1.50
1.0	0.225	0.27	0.51	0.74	0.99	1.23	1.72
1.0	0.250	0.39	0.62	0.86	1.09	1.32	1.80
1.0	0.300	0.61	0.82	1.03	1.25	1.47	1.91
1.0	0.350	0.82	1.00	1.18	1.38	1.58	1.99
1.0	0.400	1.03	1.17	1.33	1.50	1.68	2.07
1.0	0.500	1.50	1.56	1.64	1.74	1.88	2.19
2.0	0.200	0.00	0.25	0.50	0.75	1.00	1.50
2.0	0.225	0.27	0.51	0.76	1.00	1.24	1.74
2.0	0.250	0.40	0.63	0.87	1.12	1.36	1.84
2.0	0.300	0.62	0.85	1.08	1.30	1.54	2.00
2.0	0.350	0.85	1.06	1.27	1.49	1.70	2.15
2.0	0.400	1.09	1.27	1.47	1.67	1.87	2.29
2.0	0.500	1.69	1.81	1.94	2.09	2.24	2.58

Table 8.5:
Normalised stress intensity factor $K'_{I\,appl} = f(\delta'_{00}, K'_{I\,tip}, a/W)$
for $a_0/W = 0.2$ and $m = 1$.

δ^*_{00}	a_0/a	$K^*_{I\,tip} = 0.0$	0.25	0.5	0.75	1.0	1.5	2.0	3.0
0.25	1.00	0.00	0.25	0.50	0.75	1.00	1.50	2.00	3.00
0.25	0.95	0.30	0.51	0.72	0.94	1.17	1.63	2.11	3.08
0.25	0.90	0.40	0.68	0.77	0.98	1.19	1.64	2.11	3.08
0.25	0.80	0.52	0.65	0.81	1.00	1.21	1.64	2.11	3.08
0.25	0.70	0.59	0.68	0.83	1.01	1.21	1.64	2.12	3.08
0.25	0.50	0.67	0.72	0.85	1.01	1.22	1.65	2.12	3.08
0.25	0.30	0.70	0.73	0.86	1.02	1.22	1.65	2.12	3.08
0.25	0.01	0.72	0.74	0.86	1.02	1.22	1.65	2.12	3.08
0.5	1.00	0.00	0.25	0.50	0.75	1.00	1.50	2.00	3.00
0.5	0.95	0.30	0.53	0.76	0.99	1.23	1.70	2.18	3.14
0.5	0.90	0.42	0.63	0.84	1.06	1.28	1.74	2.20	3.15
0.5	0.80	0.57	0.74	0.92	1.12	1.33	1.77	2.21	3.16
0.5	0.70	0.66	0.80	0.97	1.16	1.35	1.78	2.22	3.16
0.5	0.50	0.78	0.88	1.02	1.19	1.38	1.79	2.23	3.16
0.5	0.30	0.87	0.93	1.05	1.20	1.39	1.79	2.23	3.16
0.5	0.01	0.92	0.96	1.07	1.21	1.39	1.79	2.23	3.16
1.0	1.00	0.00	0.25	0.50	0.75	1.00	1.50	2.0	3.0
1.0	0.95	0.32	0.55	0.79	1.02	1.27	1.75	2.23	3.20
1.0	0.90	0.43	0.65	0.89	1.12	1.35	1.82	2.28	3.24
1.0	0.80	0.58	0.79	1.00	1.22	1.44	1.89	2.34	3.27
1.0	0.70	0.69	0.88	1.08	1.28	1.49	1.92	2.37	3.30
1.0	0.50	0.83	1.00	1.17	1.36	1.55	1.96	2.39	3.30
1.0	0.30	0.93	1.06	1.22	1.40	1.59	1.98	2.41	3.31
1.0	0.01	1.00	1.11	1.25	1.42	1.60	1.99	2.42	3.31
2.0	1.00	0.00	0.25	0.50	0.75	1.00	1.50	2.0	3.0
2.0	0.95	0.32	0.55	0.80	1.04	1.29	1.78	2.26	3.25
2.0	0.90	0.43	0.67	0.91	1.15	1.39	1.87	2.35	3.32
2.0	0.80	0.59	0.82	1.05	1.28	1.51	1.98	2.44	3.39
2.0	0.70	0.7	0.92	1.14	1.36	1.59	2.04	2.50	3.43
2.0	0.50	0.85	1.05	1.26	1.47	1.69	2.12	2.57	3.50
2.0	0.30	0.94	1.13	1.33	1.53	1.74	2.16	2.61	3.51
2.0	0.01	1.00	1.18	1.38	1.57	1.77	2.19	2.62	3.51
4.0	1.00	0.00	0.25	0.50	0.75	1.00	1.50	2.0	3.0
4.0	0.95	0.32	0.55	0.81	1.06	1.30	1.80	2.28	3.28
4.0	0.9	0.44	0.68	0.92	1.17	1.42	1.90	2.39	3.37
4.0	0.8	0.60	0.85	1.08	1.32	1.56	2.04	2.52	3.48
4.0	0.7	0.72	0.94	1.18	1.42	1.65	2.12	2.60	3.55

4.0	0.5	0.85	1.09	1.32	1.54	1.77	2.23	2.70	3.63
4.0	0.3	0.95	1.18	1.39	1.62	1.85	2.30	2.76	3.68
4.0	0.01	1.00	1.22	1.44	1.66	1.89	2.33	2.78	3.71

Table 8.6:
Normalised stress intensity factor $K^*_{I\,appl} = f(\delta^*_{00}, K^*_{I\,tip}, a_0/a)$ for m = 1.

The following program provides the stress intensity factor $K_{I\,appl}$ for given values of δ'_{00} (DEL0), a/W (ADW) and $K_{I\,tip}$ (TIP). The resulting stress intensity factor $K_{I\,appl}$ is named APPL. The subroutine RUF reads the content of table 8.1.
The subroutines IBCIEU, ICSCCU and ICSEVU are spline-routines provided by the IMSL program library.

```
      IMPLICIT REAL*8 (A-H,O-Z)
      CALL RUF
      DEL0=0.4D0
      TIP=1.4970D0
      ADW=0.6D0
      CALL FUNC(DEL0,ADW,TIP,APPL)
      WRITE(6,100) TIP,APPL
  100 FORMAT(1H 6F9.4)
      STOP
      END
      ********************************************************
      SUBROUTINE RUF
      IMPLICIT REAL*8 (A-H,O-Z)
      DIMENSION D(5,7),E(5,7),F(5,7),G(5,7)
      COMMON D,E,F,G
      OPEN (10,FILE='TSO042.TEST.DATA(TABLE81)',STATUS='SHR')
      REWIND 10
      READ(10,*,END=70) D(1,1),D(2,1),D(3,1),D(4,1),D(5,1)
      READ(10,*,END=70) D(1,2),D(2,2),D(3,2),D(4,2),D(5,2)
      READ(10,*,END=70) D(1,3),D(2,3),D(3,3),D(4,3),D(5,3)
      READ(10,*,END=70) D(1,4),D(2,4),D(3,4),D(4,4),D(5,4)
      READ(10,*,END=70) D(1,5),D(2,5),D(3,5),D(4,5),D(5,5)
      READ(10,*,END=70) D(1,6),D(2,6),D(3,6),D(4,6),D(5,6)
      READ(10,*,END=70) D(1,7),D(2,7),D(3,7),D(4,7),D(5,7)
      READ(10,*,END=70) E(1,1),E(2,1),E(3,1),E(4,1),E(5,1)
      READ(10,*,END=70) E(1,2),E(2,2),E(3,2),E(4,2),E(5,2)
      READ(10,*,END=70) E(1,3),E(2,3),E(3,3),E(4,3),E(5,3)
      READ(10,*,END=70) E(1,4),E(2,4),E(3,4),E(4,4),E(5,4)
      READ(10,*,END=70) E(1,5),E(2,5),E(3,5),E(4,5),E(5,5)
      READ(10,*,END=70) E(1,6),E(2,6),E(3,6),E(4,6),E(5,6)
      READ(10,*,END=70) E(1,7),E(2,7),E(3,7),E(4,7),E(5,7)
      READ(10,*,END=70) F(1,1),F(2,1),F(3,1),F(4,1),F(5,1)
      READ(10,*,END=70) F(1,2),F(2,2),F(3,2),F(4,2),F(5,2)
      READ(10,*,END=70) F(1,3),F(2,3),F(3,3),F(4,3),F(5,3)
      READ(10,*,END=70) F(1,4),F(2,4),F(3,4),F(4,4),F(5,4)
      READ(10,*,END=70) F(1,5),F(2,5),F(3,5),F(4,5),F(5,5)
      READ(10,*,END=70) F(1,6),F(2,6),F(3,6),F(4,6),F(5,6)
      READ(10,*,END=70) F(1,7),F(2,7),F(3,7),F(4,7),F(5,7)
      READ(10,*,END=70) G(1,1),G(2,1),G(3,1),G(4,1),G(5,1)
      READ(10,*,END=70) G(1,2),G(2,2),G(3,2),G(4,2),G(5,2)
      READ(10,*,END=70) G(1,3),G(2,3),G(3,3),G(4,3),G(5,3)
      READ(10,*,END=70) G(1,4),G(2,4),G(3,4),G(4,4),G(5,4)
      READ(10,*,END=70) G(1,5),G(2,5),G(3,5),G(4,5),G(5,5)
      READ(10,*,END=70) G(1,6),G(2,6),G(3,6),G(4,6),G(5,6)
      READ(10,*,END=70) G(1,7),G(2,7),G(3,7),G(4,7),G(5,7)
   70 CONTINUE
      RETURN
      END
      ********************************************************
      SUBROUTINE SPLINE(DEL0,ADW,TIP,WERT)
      IMPLICIT REAL*8 (A-H,O-Z)
```

```
      DIMENSION D(5,7),E(5,7),F(5,7),G(5,7),Y(7)
      DIMENSION X(5),FL(1,7),XL(1),YL(1),WK(25)
      COMMON D,E,F,G
      IFD=5
      NX=5
      NY=7
      NXL=1
      NYL=1
      X(1)=0.0D0
      X(2)=0.25D0
      X(3)=0.5D0
      X(4)=1.0D0
      X(5)=1.5D0
      Y(1)=0.5D0
      Y(2)=0.525D0
      Y(3)=0.55D0
      Y(4)=0.6D0
      Y(5)=0.65D0
      Y(6)=0.7D0
      Y(7)=0.75D0
      XL(1)=TIP
      YL(1)=ADW
      IFLD=1
      IF(DABS(DEL0-0.25D0).LT.1.D-2) GOTO 40
      IF(DABS(DEL0-0.50D0).LT.1.D-2) GOTO 41
      IF(DABS(DEL0-1.00D0).LT.1.D-2) GOTO 42
      IF(DABS(DEL0-2.00D0).LT.1.D-2) GOTO 43
   40 CALL IBCIEU(D,IFD,X,NX,Y,NY,XL,NXL,YL,NYL,FL,IFLD,WK,IER)
      GOTO 44
   41 CALL IBCIEU(E,IFD,X,NX,Y,NY,XL,NXL,YL,NYL,FL,IFLD,WK,IER)
      GOTO 44
   42 CALL IBCIEU(F,IFD,X,NX,Y,NY,XL,NXL,YL,NYL,FL,IFLD,WK,IER)
      GOTO 44
   43 CALL IBCIEU(G,IFD,X,NX,Y,NY,XL,NXL,YL,NYL,FL,IFLD,WK,IER)
      GOTO 44
   44 CONTINUE
      WERT=FL(1,1)
      RETURN
      END
      *******************************************************
      SUBROUTINE FUNC(DEL0,ADW,TIP,APPL)
      IMPLICIT REAL*8 (A-H,O-Z)
      DIMENSION X(4),Y(4),C(3,3),U(1),S(1)
      NX=4
      IC=3
      M=1
      X(1)=0.25D0
      X(2)=0.50D0
      X(3)=1.00D0
      X(4)=2.00D0
      X1=X(1)
      X2=X(2)
      X3=X(3)
      X4=X(4)
      CALL SPLINE(X1,ADW,TIP,WERT1)
      CALL SPLINE(X2,ADW,TIP,WERT2)
      CALL SPLINE(X3,ADW,TIP,WERT3)
```

```
CALL SPLINE(X4,ADW,TIP,WERT4)
Y(1)=WERT1
Y(2)=WERT2
Y(3)=WERT3
Y(4)=WERT4
U(1)=DEL0
CALL ICSCCU(X,Y,NX,C,IC,IER)
CALL ICSEVU(X,Y,NX,C,IC,U,S,M,IER)
APPL=S(1)
RETURN
END
```